

OPEN ACCESS

Pt-Catalyzed D-Glucose Oxidation Reactions for Glucose Fuel Cells

To cite this article: Ji Huang *et al* 2021 *J. Electrochem. Soc.* **168** 064511

View the [article online](#) for updates and enhancements.



Pt-Catalyzed D-Glucose Oxidation Reactions for Glucose Fuel Cells

Ji Huang,¹ Philipp Simons,² Yusuke Sunada,¹ Jennifer L. M. Rupp,^{2,3} and Shunsuke Yagi^{1,*} 

¹Institute of Industrial Science, The University of Tokyo, 4-6-1 Komaba, Meguro-ku, Tokyo 153-8505, Japan

²Department of Materials Science and Engineering, Massachusetts Institute of Technology, Cambridge, MA 02139, United States of America

³Department of Electrical Engineering and Computer Science, Massachusetts Institute of Technology, Cambridge, MA 02139, United States of America

The Pt-catalyzed D-glucose oxidation reaction in neutral electrolytes was investigated for implantable power applications. A reaction mechanism involving two possible oxidation pathways, namely direct and OH_{ads}-mediated oxidation, was proposed based on the mass change during electrochemical measurement. PtPd and Pt₂Pd were synthesized as anodic catalysts by a solvothermal method, and single-chamber glucose-air fuel cells using a neutral aqueous electrolyte were prototyped successfully. Higher fuel cell performance was achieved with the PtPd catalyst, with a maximum power density of 27.6 μW cm⁻² and open-circuit voltage of 0.616 V. Collectively, the present study contributes to maximize the performance of glucose fuel cells.

© 2021 The Author(s). Published on behalf of The Electrochemical Society by IOP Publishing Limited. This is an open access article distributed under the terms of the Creative Commons Attribution 4.0 License (CC BY, <http://creativecommons.org/licenses/by/4.0/>), which permits unrestricted reuse of the work in any medium, provided the original work is properly cited. [DOI: 10.1149/1945-7111/ac0949]



Manuscript submitted April 29, 2021; revised manuscript received May 20, 2021. Published June 16, 2021.

Supplementary material for this article is available [online](#)

Glucose fuel cells have received increased attention in recent years for both external and implantable applications.^{1–5} As fuel cells, they show great potential for generating green electricity through biomass conversion, since glucose is a dominant component of biomass products. In addition, the standard Gibbs energy change of complete glucose oxidation to CO₂ and H₂O is negatively high at approximately -2,870 kJ mol⁻¹, corresponding to the maximum theoretical glucose fuel cell voltage of approximately 1.24 V.⁶ Glucose fuel cells can help lead the energy transition away from greenhouse gas emitting fossil fuels and towards renewable energy sources. Another field of application is the use-case as implantable fuel cells. For instance, glucose fuel cells promise to harvest energy that is readily and abundantly available inside the human body and can therefore be used as power implantable biomedical devices.¹

To rationally design and engineer glucose fuel cells for both external and implantable applications, it is paramount to understand the catalytic processes that occur at both electrodes, and to develop catalysts that can perform well at temperatures close to room temperature. Because the glucose oxidation reaction is complex and the overpotential is high, the anode is a critical component of the glucose fuel cell.¹ To date, many studies have focused on employing enzymes such as glucose oxidase for the catalysis of the glucose oxidation reaction.^{3,7,8} This enzyme has the benefit of being a highly selective and active catalyst and enzymatic glucose fuel cells have been successfully implanted in rats.^{7,8} However, enzymes deactivate easily and lack long-term stability when they are isolated and stabilized on an electrode, leading to short glucose fuel cell lifetimes of the order of several weeks. In addition, they show relatively poor charge transfer behavior, owing to the complexity of the enzyme molecules. Thus, abiotic catalysts have gained significant attention in recent years as a strategy to overcome these disadvantages. Abiotic catalysts include pure or alloyed noble metals that are often modified on carbon in the form of carbon nanotubes or activated carbon.^{1,9–15} These catalysts exhibit long-term stability together with facile charge transfer. In addition, abiotic catalysts can be thermally sterilized without any loss of catalytic activity. Nevertheless, the power density of abiotic glucose fuel cells is not as sufficient^{14,15} as that of enzymatic glucose fuel cells to allow practical application. This relatively low power density in abiotic glucose fuel cells is attributed to two main factors, namely the high

overpotentials and sluggish kinetics of the complex glucose oxidation reaction.¹ Therefore, catalysts with higher activities are required.

To design highly active catalysts, it is necessary to understand the glucose oxidation reaction in greater detail. In their spectroscopic study, Beden et al. reported that gluconic acid was obtained as the final main product through the oxidation of weakly adsorbed intermediates formed by dehydrogenation of the anomeric carbon of glucose.¹⁶ However, questions about the mechanism of this process remain unanswered, which limits further improvement. For example, generally, an oxidation peak is observed during a positive potential sweep; however, an oxidation peak is also observed during a negative potential sweep for the working electrode of glucose fuel cells. This suggests the presence of several adsorption/desorption processes of the intermediate species, which, however, is not yet fully understood. Therefore, in this study, we investigate the mechanism of the glucose (D-glucose) oxidation reaction on Pt-based catalysts of high catalytic activity by cyclic voltammetry and electrochemical quartz crystal microbalance (EQCM) measurements to clarify the adsorption/desorption behavior of these intermediate species. In addition, the effects of alloying Pt with Pd to further enhance the catalytic activity were discussed, based on the glucose oxidation mechanism described later.

Experimental

Preparation of the catalysts.—All reagents other than commercial platinum on graphitized carbon (Pt/C, 20% Pt/Vulcan XC72, Sigma-Aldrich Co. LLC.) were purchased from Nacalai Tesque, Inc. and used without further purification. To synthesize the Pt₂Pd and PtPd catalysts, 0.2 ml of 8 wt.% H₂PtCl₆ aqueous solution, prepared by dissolving H₂PtCl₆ in deionized water, 2 g of KOH, and 3.5 or 7 mg of PdCl₂ were mixed and dissolved in a mixed solvent containing 24 ml of N,N-dimethylformamide (DMF) and 16 ml of ethylene glycol (EG).¹⁷ After stirring the solution for 12 h, the resultant viscous solution was transferred into a 100 ml Teflon-lined autoclave. The autoclave was maintained at 170 °C for 8 h and then cooled to room temperature. The black products were collected by centrifugation, washed threefold with ethanol and deionized water, and subsequently dried at 60 °C overnight.

Preparation of the working electrode.—K⁺-ion-exchanged Nafion solution was prepared as a binder by mixing 10 ml of 5 wt % Nafion (Sigma-Aldrich Co. LLC.) and 5 ml of 0.1 M KOH aqueous solution

*Electrochemical Society Member.

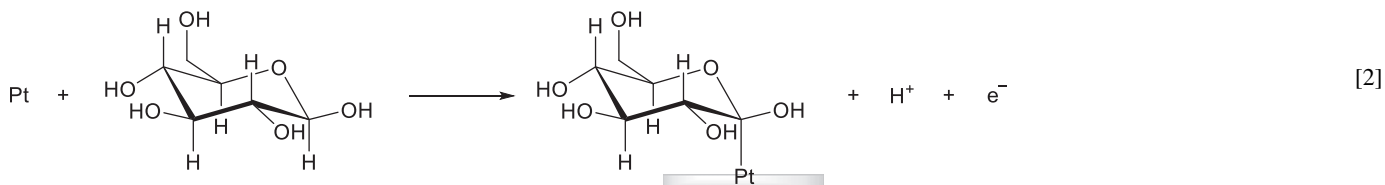
^zE-mail: syagi@iis.u-tokyo.ac.jp

(Nacalai Tesque, Inc.). In a typical catalyst ink preparation, 10 mg of catalyst was mixed with 2 mg of carbon black (acetylene black), 1.94 ml of tetrahydrofuran (THF, Nacalai Tesque, Inc.), and 60 ml of the K^+ -ion-exchanged Nafion aqueous solution in a glass bottle and subsequently ultrasonicated for 10 min. A working electrode for cyclic voltammetry was prepared by dropping 6.4 μl of the catalyst ink on the surface of a glassy carbon rotating disk electrode (GC-RDE, diameter: 4 mm). The anode for a single-chamber fuel cell was prepared by dropping 46 μl of the catalyst ink on the surface of a circular carbon paper, 13 mm in diameter. On the other hand, the cathode for the single-chamber fuel cell was prepared by dropping 64 μl of the Pt/C catalyst ink on the surface of a gas diffusion layer (GDL, GDL-39BC, MFC Technology Inc.) 13 mm in diameter. The modified electrodes were then dried at 50 $^{\circ}\text{C}$ in air for more than 30 min.

Characterization.—The morphologies and chemical compositions of the catalysts were characterized by scanning electron microscopy (SEM) and energy-dispersive X-ray spectroscopy (EDX) (JSM-6010LA, JEOL Ltd.). The structure of the catalysts was analyzed by X-ray diffraction (XRD; Ultima IV, Rigaku Co., Ltd.) with a molybdenum X-ray tube.

Electrochemical measurements.—Cyclic voltammetry was conducted using a three-electrode setup with a rotating ring-disk electrode system (RRDE-3A, BAS Inc.) and a potentiostat (ALS705EY, BAS Inc.) at 1,600 rpm and 10 mV s^{-1} . The modified GC-RDE, Pt spring electrode, and Ag/AgCl (sat. KCl) electrode were used as the working, counter, and reference electrodes, respectively. Electrochemical measurements were performed using an electrochemical quartz crystal microbalance (EQCM) attached to a resonance frequency counter (QCM922A, SEIKO EG&G Co., Ltd.) and a potentiostat (VSP-300, BioLogic Sciences Instruments). All the potentials measured were converted to the value vs reversible hydrogen electrode (RHE) using the equation:

$$E(\text{V vs RHE}) = E(\text{V vs Ag/AgCl, sat. KCl}) + 0.05916 \text{ pH} + 0.197 \text{ V} \quad [1]$$



All current densities were obtained using the geometric areas of the working electrode parts exposed to electrolytes (GC-RDE: $0.2 \times 0.2 \times \pi \text{ cm}^2$, QCM electrode: $0.25 \times 0.25 \times \pi \text{ cm}^2$, and fuel cell electrode: $0.65 \times 0.65 \times \pi \text{ cm}^2$).

Results and Discussion

The typical cyclic voltammograms for a GC-RDE modified with the Pt/C catalyst, measured in 0.1 M Na_2SO_4 aqueous electrolyte with different glucose concentrations, are presented in Fig. 1a. While no significant peaks were observed with the glucose-free electrolyte, three anodic peaks were observed during the positive potential sweep at approximately 0.4, 0.75, and 0.95 V vs RHE. The current density increased with increasing glucose concentration, and therefore, these peaks correspond to the oxidation of glucose or its oxidative intermediates. As can be seen in the glucose-free cyclic voltammogram, a relatively strong capacitive behavior is observed, which offsets the current density to positive during the positive potential sweep and to negative during the negative potential sweep in this system. Therefore, even if the current density drops below zero after the reversal to the negative potential sweep, the oxidation

of glucose continues. By considering the glucose-free voltammogram as a baseline, anodic peaks (declines in cathodic current) were also observed during the negative potential sweep at approximately 0.5 and 0.75 V vs RHE in the presence of glucose. The emergence of anodic peaks during the negative potential sweep suggests that oxidative intermediates were adsorbed on the catalyst surface during the positive potential sweep, thereby inhibiting the oxidation reaction, while desorption of the intermediates occurred during the negative potential sweep. However, the details of these processes remain unclear.

We therefore proceeded to investigate the adsorption/desorption behavior by measuring the current density and corresponding mass change of the Pt electrode using an EQCM,^{18–20} as shown in Fig. 1b. The shape of the voltammogram differed slightly from that shown in Fig. 1a because of the difference in the electrodes and potential ranges (a: GC-RDE modified with Pt/C rotated at 1,600 rpm up to 1.3 V vs RHE and b: Pt-QCM electrode without rotation up to 1.1 V vs RHE to avoid the effect of the oxygen evolution reaction). Nevertheless, it is evident that the mass decreased during the negative potential sweep and increased during the positive potential sweep, suggesting that desorption occurred during the negative potential sweep and adsorption occurred during the positive potential sweep. The mass change below 0.4 V vs RHE is much larger than that above 0.4 V vs RHE during both the negative and positive potential sweeps.

In detail, the mass change per one mole of electrons transferred was calculated in several potential ranges, as shown in Table I. During the positive potential sweep, the mass change was $+167.9 \text{ g mol}^{-1}$ in the potential range of 0.1–0.2 V vs RHE, which is similar to the molecular weight of glucose (180 g mol^{-1}). This result suggests that the oxidative adsorption of glucose via one-electron reaction mainly occurs at 0.1–0.2 V vs RHE during the positive potential sweep. This well agrees with the conclusion derived by Beden et al., from their spectroscopic study, that an adsorbed intermediate was formed on Pt by dehydrogenation of a more reactive axial H atom bonded to the anomeric carbon of glucose in the β -D-glucopyranose form at lower potentials as follows:¹⁶

Furthermore, Beden et al. reported that the adsorbed dehydrogenated glucose is further oxidized to the weakly adsorbed δ -gluconolactone, and is finally oxidized to gluconic acid through C–O–C bond breakage. Thus, we further discuss the results based on this report: In the potential range of 0.2–0.4 V vs RHE, the mass change decreased to $+49.6 \text{ g mol}^{-1}$ but was still positive. Therefore, the oxidation of the adsorbed intermediate (dehydrogenated glucose), possibly to δ -gluconolactone, occurred in addition to the dehydrogenation of glucose in the potential range of 0.2–0.4 V vs RHE. Notably, an anodic peak is observed at approximately 0.3 V vs RHE in Fig. 1b, suggesting that the oxidation of the adsorbed dehydrogenated glucose is slower than the oxidative adsorption of the dehydrogenated glucose, which results in a lack of active Pt sites where the dehydrogenated glucose can be adsorbed. Hence, the subsequent oxidation of the adsorbed dehydrogenated glucose is the rate-determining step. This result is also supported by the fact that the smallest mass change ($+6.49 \text{ g mol}^{-1}$) was detected in the potential range of 0.4–0.8 V vs RHE, despite the largest current density. The mass did not change significantly because the empty active Pt sites formed by further oxidation of the adsorbed glucose to δ -gluconolactone and gluconic acid were immediately occupied by

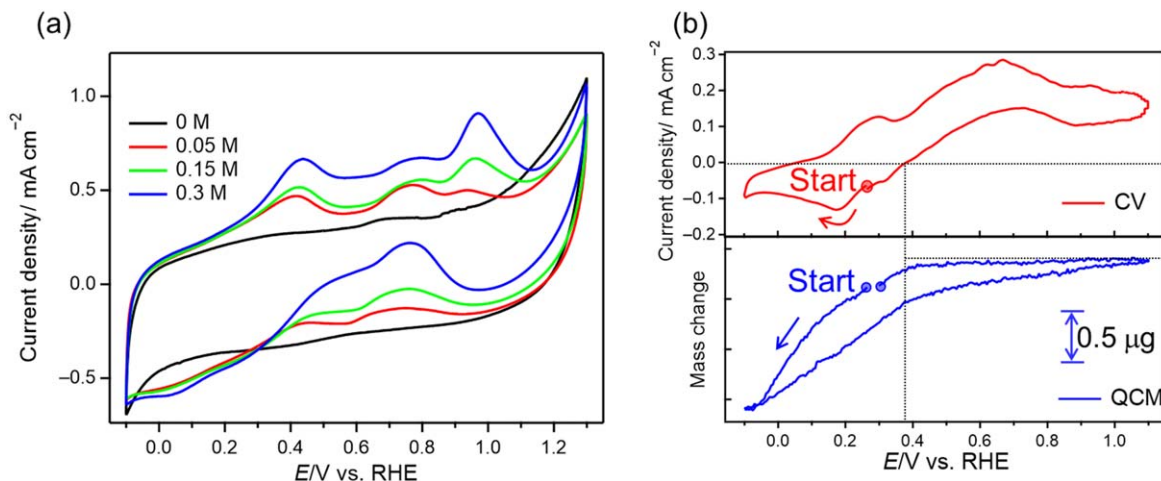


Figure 1. (a) Cyclic voltammograms for a GC-RDE modified with commercial Pt/C catalyst measured at 1,600 rpm and 10 mV s⁻¹ in N₂-saturated 0.1 M Na₂SO₄ aqueous electrolyte without glucose (black curve) and with 0.05 M (red curve), 0.15 M (green curve), and 0.3 M (blue curve) glucose. (b) Cyclic voltammogram (red curve) at the 5th cycle for the Pt-QCM electrode measured at 5 mV s⁻¹ in N₂-saturated 0.1 M Na₂SO₄ aqueous electrolyte containing 0.1 M glucose and the corresponding mass change (blue curve) of the Pt-QCM electrode.

Table I. Electrical quantity, Q , and mass change per one mole of electrons transferred, Δm , calculated from the EQCM result shown in Fig. 1b.

| | Positive potential sweep | | | | Negative potential sweep | | | | |
|-------------------------------|--------------------------|---------|---------|---------|--------------------------|---------|---------|----------|----------|
| | Potential range/V vs RHE | 0.1–0.2 | 0.2–0.4 | 0.4–0.8 | 0.8–1.1 | 1.1–0.8 | 0.8–0.4 | 0.4–0.26 | 0.26–0.1 |
| Q/mC | 0.121 | 0.896 | 3.67 | 0.836 | 1.33 | 1.67 | -0.189 | -1.43 | |
| $\Delta m/g \text{ mol}^{-1}$ | +167.9 | +49.6 | +6.59 | +16.8 | -1.39 | -2.71 | -83.9 | -82.0 | |

the new dehydrogenated glucose, resulting in a steady adsorption state. Based on the above, if the oxidative adsorption of glucose is fast enough to provide sufficient reactant (dehydrogenated glucose), the current density should not be lowered with an increase in the potential, where the driving force for the oxidation of the adsorbed dehydrogenated glucose increases. However, a decline in the current density (broad anodic peak) is observed at 0.4–0.8 V vs RHE, which cannot be explained by only considering the positive sweep voltammogram. Indeed, the characteristic anodic peak during the “negative” potential sweep in the same potential region provides further insight.

Generally, the anodic current increases with increasing potential, and this abnormal anodic peak (current increase) during the negative potential sweep suggests that active Pt sites are occupied by other species (i.e., OH_{ads}) through the oxidation of OH⁻ ions. By considering the top of the anodic peak during the negative potential sweep, the oxidative adsorption of OH⁻ ions becomes preferential above 0.7 V vs RHE and intensifies with increasing potential. Normally, the increase in the occupation of active Pt sites by OH_{ads} lowers the current density for the direct oxidation of the adsorbed glucose. However, the significantly small anodic peak in Fig. 1b and relatively large peak in Fig. 1a in the range 0.9–1.0 V vs RHE, observed only during the positive potential sweep, suggest that OH_{ads} can also promote the indirect oxidation of glucose, possibly by C–O–C bond breakage.¹⁶ Furthermore, once the adsorbed glucose was consumed at higher potentials, most of the active Pt sites were occupied by OH_{ads}, leading to a decline in the anodic current at 0.9–1.0 V vs RHE. However, the amount of OH_{ads} decreases by the subsequent negative potential sweep, and a refreshed Pt surface appears, providing active sites for glucose oxidation. In this way, an increase in the current density corresponding to direct glucose oxidation is observed during the negative potential sweep.

Table I shows also the mass changes during the negative potential sweep. Above 0.4 V vs RHE, the mass change is very small (approximately -2 g mol⁻¹), even though there is an anodic peak in the potential range of 0.8–0.4 V vs RHE, suggesting the steady

oxidative adsorption of glucose and subsequent desorption of δ -gluconolactone. Below 0.4 V vs RHE, the mass change is approximately -80 g mol⁻¹ (smaller than the molecular weight of glucose: 180 g mol⁻¹), which suggests that the reductive desorption of the dehydrogenated glucose dominates the current, but that reductive hydrogen adsorption also occurs.

Based on the above results and discussion, the oxidation of glucose can be divided into two pathways, namely direct and OH_{ads}-mediated oxidation. Both pathways start from the oxidative dehydrogenation of glucose, resulting in the adsorption of glucose on the Pt surface. The direct oxidation of the adsorbed glucose to weakly adsorbed δ -gluconolactone and gluconic acid then proceeds, while oxidation aided by OH_{ads} also occurs at higher potentials (above 0.8 V vs RHE), where sufficient OH_{ads} is generated. Thus, an increase in the amount of OH_{ads} is a possible strategy to promote glucose oxidation at higher potentials.

PtPd and Pt₂Pd particles were synthesized and evaluated against a commercial Pt/C catalyst because of the easier formation of OH_{ads}, O_{ads}, and H₂O_{ads} on Pd at lower potentials²¹ (strictly, this also depends on the alloy configuration²²). As can be seen in the X-ray diffraction (XRD) patterns in Fig. 2a, the bimetallic catalysts, PtPd and Pt₂Pd, both comprise face-centered cubic (fcc) structures. Moreover, the PtPd and Pt₂Pd particles do not differ significantly and are smaller than 1 μ m, as can be seen in the scanning electron microscopy (SEM) images in Fig. 2b and elemental analysis results in Fig. S1 (available online at stacks.iop.org/JES/168/064511/mmedia).

The electrocatalytic performances of the bimetallic catalysts, PtPd and Pt₂Pd, for the glucose oxidation reaction were evaluated in 0.1 M Na₂SO₄ aqueous electrolytes with different concentrations of glucose under N₂ atmosphere. Typical cyclic voltammograms measured in an aqueous electrolyte containing 0.5 M glucose are shown in Fig. 3a, and for comparison, the current densities at 1 V vs RHE during positive potential sweep with various glucose concentrations are shown in Fig. 3b. As can be seen in Figs. 3a and 3b, the current densities for PtPd and Pt₂Pd are larger than that for Pt/C,

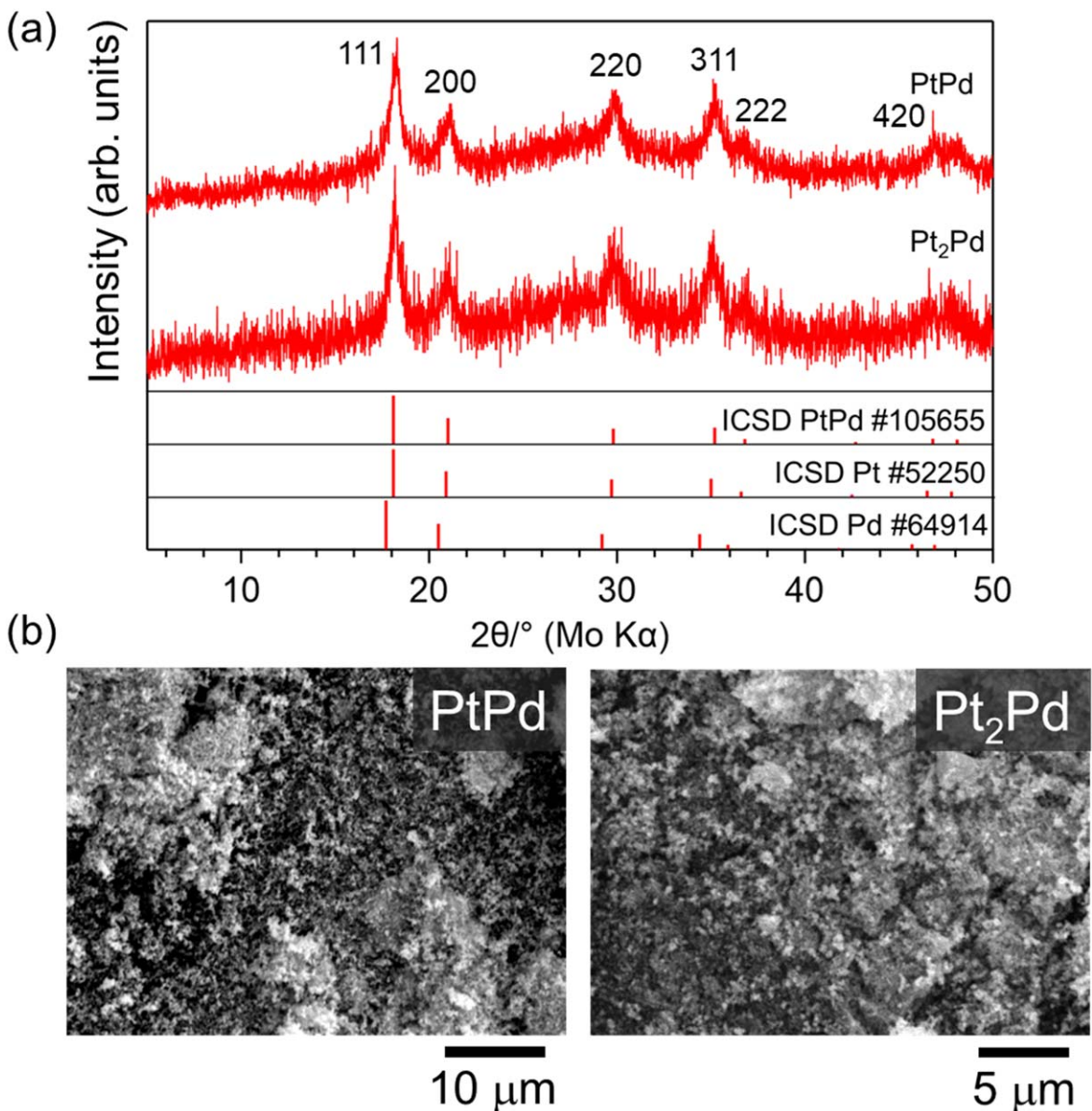


Figure 2. (a) XRD patterns and (b) SEM images of the PtPd and Pt₂Pd catalysts.

with PtPd showing the highest current density. The electrochemically active surface area (ECSA) was determined by calculating the Coulombic charge of the hydrogen underpotential deposition in a N₂-saturated 0.1 M HClO₄ aqueous electrolyte.²³ The estimated ECSAs of PtPd, Pt₂Pd, and Pt/C are 53.1 m² g⁻¹, 24.2 m² g⁻¹, and 63.7 m² g⁻¹, respectively (Fig. S2). The current densities for PtPd and Pt₂Pd are larger than that for Pt/C despite the lower ECSAs, indicating that the intrinsic catalytic activity of Pt can be improved by alloying with Pd. Specifically, the current densities at higher potentials are significantly enhanced, possibly because of the increase in the amount of OH_{ads} on the Pd surface.

Single-chamber glucose fuel cells were assembled using a N₂-saturated 0.1 M Na₂SO₄ aqueous electrolyte containing 0.5 M glucose, a Pt/C-modified GDL as the cathode catalyst, and PtPd- or Pt₂Pd-modified carbon paper as the anode, as displayed in Fig. 3c. Figures 3d and 3e show the performances of the fuel cell in air with PtPd and Pt₂Pd catalysts, respectively. The fuel cell with PtPd (Fig. 3d) exhibited a maximum power density of 27.6 μW cm⁻², an open-circuit voltage of 0.616 V, and a short-circuit current density of 0.239 mA cm⁻², which surpass the corresponding properties of the fuel cell with Pt₂Pd (Fig. 3e: Maximum power density, 9.84 μW cm⁻²; open-circuit voltage,

0.354 V; and short-circuit current, density 0.095 mA cm⁻²). It should be noted that the cell voltage is determined by the difference between the anode potential and the cathode potential. Therefore, the lowering in the cell voltage corresponds to the increase in the anode potential (and the decrease in the cathode potential), where the indirect glucose oxidation through OH_{ads} becomes predominant. These results agree with our prediction that PtPd provides more active sites for OH_{ads} than Pt₂Pd, thereby promoting glucose oxidation. The performance is comparable to that of other systems using enzyme-modified electrodes in neutral electrolytes;¹³ however, the same procedure should be adopted for the accurate comparison of catalysts because the catalytic activity and cell performance can be changed by many factors, such as the type of electrolyte and electrodes, pH, temperature, and electrode modification procedure.

Conclusions

Glucose fuel cells are of interest for clean energy storage and implantable applications. Despite the promise and proofs of concepts, the oxidation mechanism of glucose remains unclear. In this work, the mechanism of the Pt-catalyzed glucose oxidation reaction

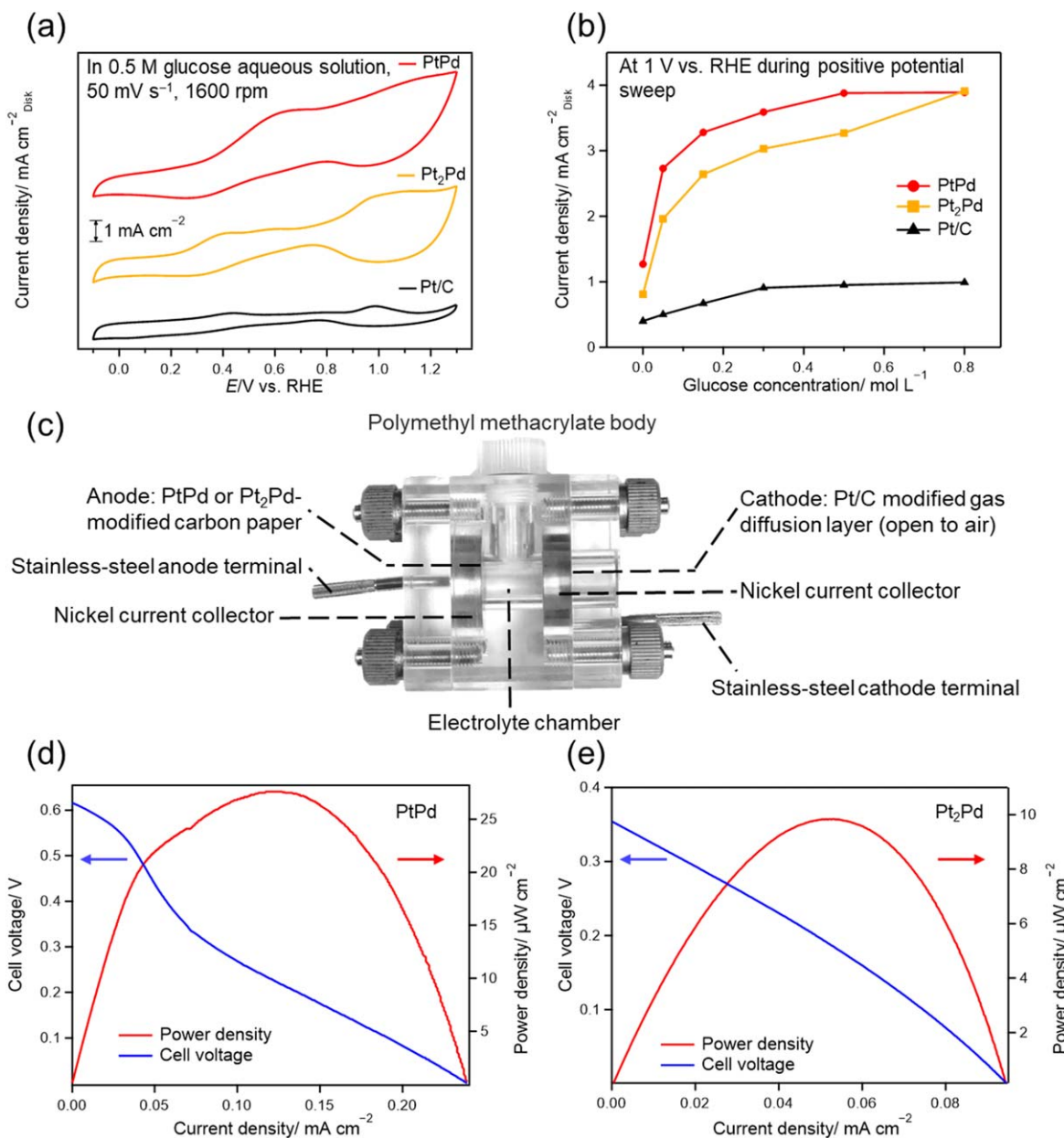


Figure 3. (a) Typical cyclic voltammograms measured under N₂ atmosphere for PtPd, Pt₂Pd, and Pt/C catalysts in a 0.1 M Na₂SO₄ aqueous electrolyte containing 0.5 M glucose at 50 mV s⁻¹ after three cycles. (b) Current densities at 1 V vs RHE during positive potential sweep with various glucose concentrations. (c) Picture of a single-chamber glucose fuel cell prototype. (d) Cell voltage and power density in air as functions of cell current density for PtPd. (e) Cell voltage and power density in air as functions of cell current density for Pt₂Pd.

was discussed based on the EQCM results. The oxidation of glucose was designated as two pathways. Both pathways start from the adsorption of glucose through oxidative dehydrogenation, which occurs even at lower potentials above 0.1 V vs RHE. The direct oxidation of the adsorbed glucose occurs over a wide range of potentials, while the indirect oxidation proceeds at higher potentials above 0.8 V vs RHE with the aid of OH_{ads}. The anodic peak during the negative potential sweep was attributed to the formation of a refreshed catalyst surface through the reductive desorption of OH_{ads}. The alloying of Pt with Pd improved the electrocatalytic activity for the glucose oxidation reaction because Pd enhances OH_{ads} formation and promotes indirect glucose oxidation. Collectively, this signifies a novel approach for the design of catalysts for glucose oxidation reaction. A single-chamber glucose fuel cell was prototyped with the PtPd catalyst and a neutral aqueous electrolyte, showing a performance comparable to that of glucose fuel cells with enzyme-modified electrodes.

Acknowledgments

This research was supported by a Grant-in-Aid for the University of Tokyo Excellent Young Researcher and a Grant-in-Aid for Scientific Research (18H03835 and 20H05180) commissioned by the Japan Society for the Promotion of Science.

ORCID

Shunsuke Yagi  <https://orcid.org/0000-0003-1675-650X>

References

- Ó. Santiago, E. Navarro, M. A. Raso, and T. J. Leo, *Appl. Energy*, **179**, 497 (2016).
- B. E. Logan, *Microbial Fuel Cells*. (Wiley, Wiley Online Library) (2008), <https://onlinelibrary.wiley.com/doi/book/10.1002/9780470258590>.
- D. Leech, P. Kavanagh, and W. Schuhmann, *Electrochim. Acta*, **84**, 223 (2012).
- S. Kerzenmacher, J. Ducr e, R. Zengerle, and F. von Stetten, *J. Power Sources*, **182**, 1 (2008).

5. S. Kerzenmacher, J. Ducré, R. Zengerle, and F. von Stetten, *J. Power Sources*, **182**, 66 (2008).
6. S. Shleev, *ChemPlusChem*, **82**, 522 (2017).
7. A. Zebda et al., *Sci. Rep.*, **3**, 1516 (2013).
8. P. Cinquin et al., *PLoS One*, **5**, e104761 (2010).
9. S. Kerzenmacher, M. Schroeder, R. Brämer, R. Zengerle, and F. von Stetten, *J. Power Sources*, **195**, 6516 (2010).
10. S. Kerzenmacher, U. Kräling, M. Schroeder, R. Brämer, R. Zengerle, and F. von Stetten, *J. Power Sources*, **195**, 6524 (2010).
11. U. P. Do, F. Seland, M. M. Maharbiz, K. Wang, Ø. Johannessen, and E. A. Johannessen, *J. Mater. Sci.*, **51**, 9095 (2016).
12. M. Frei, J. Erben, J. Martin, R. Zengerle, and S. Kerzenmacher, *J. Power Sources*, **362**, 168 (2017).
13. B. I. Rapoport, J. T. Kedzierski, and R. Sarpeshkar, *PLoS One*, **7**, e384361 (2012).
14. N. Fujiwara, S. Yamazaki, Z. Siroma, T. Ioroi, H. Senoh, and K. Yasuda, *Electrochem. Commun.*, **11**, 390 (2009).
15. K. Elouarzaki, A. Le Goff, M. Holzinger, J. Thery, and S. Cosnier, *J. Am. Chem. Soc.*, **134**, 14078 (2012).
16. B. Beden, F. Largeaud, K. B. Kokoh, and C. Lamy, *Electrochim. Acta*, **41**, 701 (1996).
17. B. Y. Xia, H. B. Wu, Y. Yan, X. W. (. D.). Lou, and X. Wang, *J. Am. Chem. Soc.*, **135**, 9480 (2013).
18. S. Yagi, M. Fukuda, T. Ichitsubo, K. Nitta, M. Mizumaki, and E. Matsubara, *J. Electrochem. Soc.*, **162**, A2356 (2015).
19. S. Yamagata, I. Takahara, M. Wang, T. Mizoguchi, and S. Yagi, *J. Alloys Compd.*, **846**, 1 (2020).
20. M. Wang and S. Yagi, *J. Alloys Compd.*, **820**, 153135 (2020).
21. X. Chen, L. P. Granda-Marulanda, I. T. McCrum, and M. T. M. Koper, *Chem. Sci.*, **11**, 1703 (2020).
22. Y.-W. Huang, T.-Y. Chou, G.-Y. Yu, and S.-L. Lee, *J. Phys. Chem. C*, **115**, 9105 (2011).
23. C. Wei, S. Sun, D. Mandler, X. Wang, S. Z. Qiao, and Z. J. Xu, *Chem. Soc. Rev.*, **48**, 2518 (2019).